Phase control of spin waves based on a magnetic defect in a one-dimensional magnonic crystal

Korbinian Baumgaertl,[1, a)] Sho Watanabe,[1] and Dirk Grundler[1, 2, b)]
[1)] *Laboratory of Nanoscale Magnetic Materials and Magnonics (LMGN), Institute of Materials (IMX), School of Engineering, Ecole Polytechnique Fédérale de Lausanne (EPFL), 1015 Lausanne, Switzerland*
[2)] *Institute of Microengineering (IMT), School of Engineering, Ecole Polytechnique Fédérale de Lausanne (EPFL), 1015 Lausanne, Switzerland*

(Dated: 22 March 2018)

Magnonic crystals are interesting for spin-wave based data processing. We investigate one-dimensional magnonic crystals (1D MCs) consisting of bistable CoFeB nanostripes separated by 75 nm wide air gaps. By adjusting the magnetic history, we program a single stripe of opposed magnetization in an otherwise saturated 1D MC. Its influence on propagating spin waves is studied via broadband microwave spectroscopy. Depending on an in-plane bias magnetic field, we observe spin wave phase shifts of up to almost π and field-controlled attenuation attributed to the reversed nanostripe. Our findings are of importance for magnetologics, where the control of spin wave phases is essential.

Information encoded in spin waves (SWs) can be transmitted and processed without moving electrical charge. This feature makes SWs promising for low power consumption in future logic devices[1,2]. Here magnonic crystals play an important role[3]. A specific approach is to encode data in the phase of SWs and use Mach-Zehnder-type interferometers as logic gates[4–6]. For this, the controlled manipulation of SW phases is essential. 360° domain walls were predicted to provide the relevant SW phase shift $\Delta\Theta$ of π [Ref.[4]]. This concept has however not yet been realized due to experimental challenges. Instead the magnetic field of a current carrying wire[5,6] was used to create an inhomogeneous effective field H_{eff} in a ferromagnet and shift the phase of backward volume spin waves[7]. The required current might however cause local heating. Recently, magnonic crystals with magnetic defects were thoroughly investigated[8–11], but defect-induced phase shifts for propagating SWs were not reported.

In this Letter, we explore a magnetic defect in one-dimensional (1D) magnonic crystals (MCs) as a phase shifter. The MCs consisted of bistable $Co_{20}Fe_{60}B_{20}$ (CoFeB) stripes separated by air gaps. By reversing the magnetization of a specific stripe in an otherwise ordered MC we find phase shifts of Damon-Eshbach-type (DE) SWs of close to π, depending on an applied magnetic field H. Also the SW amplitude is varied. Because of their high

FIG. 1. (a) Scanning electron microscopy image of the central region of MC1. Dispersion relations measured via wavevector resolved BLS (symbols) on saturated 1D MCs with p of (b) 400 and (c) 600 nm (plotted in the reduced zone scheme) at $H = 0$. Grey colors indicate stopbands. The dashed lines in (c) and (d) indicate fitted linear functions that evaluate the averaged slopes, i.e., the averaged group velocities. (d) MFM performed on a reference MC1 at $\mu_0 H = +18$ mT after saturation at -90 mT. Black (white) signals indicate stray fields, i.e., orientations of magnetization vectors along (opposite) to the applied field. Grey-scaled plot of (e) $a_{11}(H)$ and (f) $a_{21}(H)$ of MC1 for increasing H (indicated by arrows), after saturation at $\mu_0 H = -90$ mT. In (f) between H_{SW2} and H_{SW3} we assume the presence of a single magnetic defect. At H_{SW3} the SW signal undergoes an abrupt phase jump.

[a)]korbinian.baumgaertl@epfl.ch
[b)]dirk.grundler@epfl.ch

group velocities[12] and non-reciprocity[13] DE-type SWs are favorable for future magnonic applications.

The MCs [Fig. 1 (a)] were fabricated from magnetron-sputtered CoFeB with a thickness of (19 ± 2) nm deposited on an oxidized silicon substrate. The nanostripes were defined via electron beam lithography (EBL) using the negative resist hydrogen silsesquioxane (HSQ) and transferred into the magnetic film via ion beam etching. After the etching, a layer of ~ 20 nm thick HSQ remained as an isolation layer. We present data on two 1D MCs with periods $p = 400$ nm (sample MC1) and $p = 600$ nm (MC2). In both cases the air gap between stripes amounted to $g = (75 \pm 10)$ nm [Fig. 1 (a)], and the overall outer dimensions were 160 μm in x-direction and 80 μm in y-direction. The saturation magnetization $\mu_0 M_{\mathrm{s}} = 1.8$ T was extracted from ferromagnetic resonance measurements on a reference film (not shown). Dispersion relations $f(k)$ were studied on reference samples that were similar to MC1 [Fig. 1 (b)] and MC2 [Fig. 1 (c)] (f is the frequency, k is the wavevector). For this, we applied k-resolved Brillouin light scattering (BLS) on MCs in backscattering configuration following Refs.[14,15]. The laser had a wavelength 473 nm. A lens with focal length of 50 mm and f-number 2.8 was used to focus the laser to a spot diameter of few tens of micrometers. Figure 1 (b) and 1 (c) shows the resonance frequencies f (BLS peaks) recorded as a function of transferred in-plane wavevector k. The measured dispersion relations $f(k)$ consist of allowed minibands and SW stopbands (shaded in gray color), similar to magnonic bandstructures reported in Ref.[15]. For $p = 400$ nm ($p = 600$ nm) we attribute the first allowed miniband to a frequency regime ranging from 8.4 GHz to 11.3 GHz (6.7 GHz to 9.0 GHz). The second one ranges from 13.9 GHz to 14.4 GHz (11.5 GHz to 12.1 GHz).

We patterned coplanar waveguides (CPWs) on top of the MC1 and MC2 via EBL and lift-off processing of 4 nm thick evaporated Cr and 120 nm thick Au. Intentionally, a single CoFeB stripe in the center between CPW1 and CPW2 was longer by 8 μm [Fig. 1 (a)]. The CPWs allowed for excitation and detection of propagating SWs[16]. The center-to-center separation between CPW1 and CPW2 amounted to $s = 7.5$ μm. The width of the signal and ground lines of the CPWs were $w = 0.8$ μm. Using a vector network analyser we applied a radiofrequency signal with a power of ≤ -5 dBm at CPW1. The spatial profile of the exciting magnetic field of the CPW was simulated in COMSOL Multiphysics. Fast Fourier analysis of the in-plane field component showed a peak in SW excitation at $k_{\mathrm{I}} = 2.0 \cdot 10^4$ rad/cm, which is below the wavevector $k_{\mathrm{BZ}} = \frac{\pi}{p}$ of the first Brillouin zone (BZ) boundary, amounting to $7.9 \cdot 10^4$ rad/cm ($5.2 \cdot 10^4$ rad/cm) for MC1 (MC2). Scattering parameters $S_{11}(H)$ ($S_{21}(H)$) were recorded at CPW1 (CPW2), while a magnetic field H was applied in y-direction. In this work we discuss the magnitude of the scattering parameters. To extract the magnon-induced signal contribution $a_{ij} = S_{ij}(H) - S_{ij}(H_\perp)$ $(i, j = 1, 2)$, we subtracted the reference spectrum $S_{ij}(H_\perp)$ taken at $\mu_0 H_\perp = 90$ mT applied in x-direction, where SW excitation was negligible. We performed magnetic force microscopy (MFM) [Fig. 1 (d)] on a reference MC1 to estimate the reversal fields of the bistable nanostripes. The sample was first saturated at -90 mT with H collinear to the y-axis. Then the field was increased in steps of 1 mT. The short stripes forming the MC were found to reverse their magnetization direction between 5 and 15 mT. The long stripe switched at a larger field of 19 mT which we attributed to the modified shape anisotropy compared to the short stripes.

Figure 1 (e) shows $a_{11}(H)$ of MC1 for increasing H after it was saturated at $\mu_0 H = -90$ mT. The prominent dark branch indicates the SW resonance at k_{I}. Its frequency f_{res} (dark) linearly decreases with increasing H until $\mu_0 H_{\mathrm{SW1}} = 6 \pm 1$ mT. Here, the intensity of the branch reduces and its linewidth increases. The signal strength recovers at $\mu_0 H_{\mathrm{SW2}} = 16 \pm 1$ mT. Beyond $\mu_0 H_{\mathrm{SW2}}$, f_{res} increases with H. We attribute the field regime between H_{SW1} and H_{SW2} to the switching fields of stripes in close vicinity of CPW1. In Fig. 1 (f) field-dependent transmission signals $a_{21}(H)$ are summarized. a_{21} shows pronounced oscillations (black-white-black contrast) which we attribute to the interference of the spin-precession induced voltage and direct electromagnetic crosstalk between CPW1 and CPW2 following Ref.[17]. The crosstalk showed a stable phase, and the interference pattern allowed us to analyse phase differences $\Delta\Theta$ of transmitted SWs as will be presented later.

FIG. 2. (a) Grey scale plot (SAT) of $a_{21}(H)$ of MC1 for decreasing H (indicated by arrows) after $\mu_0 H = 90$ mT was applied. Green dashed lines indicate extrema $P1$ and $P2$ defined in (b). (b) Line plot of a_{21} at $H = 0$. $P1$ and $P2$ are used to extract δf and $\Delta_{\mathrm{p-p}}$. (c) Excitation spectrum of the CPW where k is in units of π/p. (d) $a_{21}(H)$ obtained in a minor loop (ML) assuming the presence of a magnetic defect. H was decreased starting from $\mu_0 H^* = 19$ mT after saturation at $\mu_0 H = -90$ mT. (e) Relative signal $\eta(H)$ of spectra ML compared to spectra SAT. (f) Frequency shift Δf between peaks P1 of SAT and ML datasets. (g) to (l) Corresponding data obtained on MC2. $\mu_0 H'^*$ amounted to -12 mT indicating a smaller coercive field of MC2. Green dashed lines in datasets (a), (d), (g) and (j) indicate the frequencies of extrema $P1$ and $P2$ as they are defined in (b).

Increasing H from 0 mT in Fig. 1 (f), the oscillations in a_{21} become weak at H_{SW1}. At H_{SW2} the oscillating signature regains a pronounced signal strength. Beyond $\mu_0 H_{\mathrm{SW3}} = 23 \pm 1$ mT in Fig. 1 (f) the signal is found to be even stronger than at $H = 0$. We attribute the regime between H_{SW2} and H_{SW3} to the configuration where all short stripes are aligned to the external field, but the long stripe is oppositely magnetized similar to Fig. 1 (d). Strikingly, at H_{SW3} not only the amplitude changes, but also a clear phase jump is seen in the oscillations, indicating an abrupt SW phase variation. We attribute this observation to the reversal of the long nanostripe. Similar characteristics were observed for MC2. Only the switching of stripes occurred at smaller field values of $\mu_0 H'_{\mathrm{SW1}} = 3$ mT, $\mu_0 H'_{\mathrm{SW2}} = 8.5$ mT and $\mu_0 H'_{\mathrm{SW3}} = 12.5$ mT [see Fig. (S1) in the supplementary material].

Based on Fig. 2 we now discuss in detail the effect of an individual magnetic defect on SW transmission in the 1D MCs. It is instructive to first present field-dependent transmission signals $a_{21,\mathrm{SAT}}(H)$ for the saturated (SAT) array. For Fig. 2 (a) we saturated MC1 at +90 mT and then decreased H in a stepwise manner down to $\mu_0 H = -4$ mT $> -\mu_0 H_{\mathrm{SW1}}$ without inducing a reversal. We find a branch containing pronounced oscillations over the full depicted field regime. Frequencies of local extrema P1 and P2 [Fig. 2 (b)] systematically shift with H as highlighted by broken lines. The envelope of the oscillating signal of Fig. 2 (b) reflects the excitation spectrum of the CPW which is displayed in the reduced zone scheme in Fig. 2 (c) ($k \leq k_{\mathrm{BZ}}$). For the following analysis we refer to Fig. 2 (b), define the peak-to-peak amplitude $\Delta_{\mathrm{p-p}}$ (signal strength) between neighbouring extrema $P1$ and $P2$, and introduce the frequency difference δf. According to Ref.[18] we calculate the group velocity following $v_{\mathrm{g}} = \frac{\partial \omega}{\partial k} = \frac{4\pi\delta f}{2\pi/s} = 2\delta f \times s$. At $H = 0$ we find $\delta f = 0.244$ GHz corresponding to $v_{\mathrm{g}} = 3.7$ km/s. This value represents the upper limit of v_{g}, considering Ref.[17] where a phase accumulation length smaller than s was encountered.

The effect of the defect was probed via a minor loop (ML) starting at a field H^* located between H_{SW2} and H_{SW3}. For the spectra displayed in Fig. 2 (d) we first saturated MC1 at -90 mT, and then applied $\mu_0 H^* = +19$ mT to reverse the short stripes but keep the long stripe oriented along the negative field direction. Thereby we programmed the magnetic defect. We highlight three discrepancies found in Fig. 2 (d) compared to (a): (i) between 12 and 19 mT less oscillations are present, (ii) the oscillation amplitudes are weaker over a broad field range, and (iii) the local extrema appear at different frequencies when measured at the same H. In the following we quantify the discrepancies in that we introduce both the relative signal strength $\eta(H) = \frac{\Delta_{\mathrm{p-p}}\ (\mathrm{ML})}{\Delta_{\mathrm{p-p}}\ (\mathrm{SAT})}$ [Fig. 2 (e)], and frequency shift $\Delta f = f_{P1}(\mathrm{ML}) - f_{P1}(\mathrm{SAT})$ [Fig. 2 (f)] evaluated at different H between peaks P1 of the ML and SAT datasets. In Fig. 2 (e), $\eta(H)$ is slightly above one at $H = 0$ and then decreases with increasing $|H|$ to a minimum value of 0.3 at H^*. This means that at 19 mT the programmed defect reduces the transmitted SW amplitude by 70 %. In Fig. 2 (f), the frequency shift $\Delta f(H)$ is zero at $H = 0$. At 19 mT, we find $\Delta f = -0.2$ GHz.

Corresponding measurements were also conducted for MC2. In Fig. 2 (g) we show $a_{21,\mathrm{SAT}}$ of MC2 for decreasing H after it was saturated at +90 mT and while the MC remained fully aligned. Again, we observed a clear branch with several oscillations. At $H = 0$ [Fig. 2 (h)] δf amounted to 0.279 GHz corresponding to $v_{\mathrm{g}} = 4.2$ km/s. Compared to MC1 [Fig. 2 (b)] a larger number of oscillations is observed. We attribute this to the excitation spectrum of the CPW in that the k_I peak now covers a broader range of the first BZ of MC2 [Fig.

FIG. 3. Estimated SW phase shifts $\Delta\Theta$ (full lines) when the long stripe is magnetized oppositely to the short stripes in (a) MC1 and (b) MC2. Phase shifts are given relative to the fully saturated MC. The dashed lines reflect model calculations based on Eq. (1).

FIG. 4. (a) Sketch of H_{eff} for $H > 0$. At the defect H enters H_{eff} with opposite sign. Thereby a well is formed. Considering a small H_{eff} in the well, the wave vector k' at the defect is larger than k to match the excitation frequency. (b) Dispersion relations sketched for different H_{eff}. The resonance frequency of regular stripe arrays is shifted upwards following $f(k, H_{\text{eff}} = +H)$, in the oppositely magnetized long stripe it shifts downwards following $f(k, H_{\text{eff}} = -H)$. Such a shift results in different wavevectors k_{I} and k' for a fixed frequency f with $\Delta k = k' - k_{\text{I}}$.

2 (i)]. In Fig. 2 (j) we show a_{21} obtained in a ML. After saturation at -90 mT a field of $\mu_0 H'^{*} = +12$ mT located between H'_{SW3} and H'_{SW2} was applied. In this regime the long stripe was assumed to be magnetized in opposite direction to both H and the short stripes. At H'^{*} the signal was small. When decreasing the field from H'^{*}, the signal increased until $H = 0$. This behaviour is analyzed by $\eta(H)$ shown for MC2 in Fig. 2 (k). η amounts to 0.4 (1.2) at H'^{*} ($H = 0$). Δf of MC2 is shown in Fig. 2 (l). We find $\Delta f = -0.2$ GHz (0 GHz) at H'^{*} ($H = 0$).

We assume that Δf is a measure of a magnetic-defect-induced phase shift accumulated by SWs going across a reversely magnetized nanostripe. In the following, we estimate the phase shift $\Delta\Theta$ that appears relative to the fully saturated MC. In a fully saturated MC, SWs leading to neighboring extrema P1 and P2 of spectra a_{21} in Fig. 2 (a) and (g) are separated by $\delta f(H)$ corresponding to a known phase shift of π. Using the relation $\Delta\Theta(H) = -\frac{\Delta f(H)}{\delta f(H)} \cdot \pi$ we estimate the field-dependent phase shifts $\Delta\Theta(H)$ in MC1 [solid line in Fig. 3 (a)] and MC2 [solid line in Fig. 3 (b)] considering $\delta f(H)$ of Fig. 2 (a) and (g), respectively. For both samples $\Delta\Theta$ is found to vary monotonously with H. For MC1 (MC2) $\Delta\Theta = 0.9\pi$ ($\Delta\Theta = 0.5\pi$) is reached at H^{*} (H'^{*}).

In the following we explain these findings with different static effective fields H_{eff} for the defect and the MC when $H \neq 0$ [Fig. 4 (a)]. H_{eff} enters the equation of motion for spin precession[19]. To facilitate the discussion we assume infinitely long nanostripes with a demagnetization factor $N_y = 0$ such that $|H_{\text{eff}}| \approx H$. For a positive magnetic field, H points parallel (antiparallel) to the static magnetization $\boldsymbol{M}$ of the short stripes (the reversed long stripe) and enters H_{eff} with positive (negative) sign. This scenario leads to a variation in $H_{\text{eff}}(x)$ as sketched in Fig. 4 (a). The defect represents a SW well. Corresponding dispersion relations $f(k)$ inside and outside the SW well are sketched in Fig. 4 (b). When SWs are transmitted between CPW1 and CPW2 at a fixed frequency f, the relevant wavevector k' in the well is different from k of the MC. Stimulated by Ref.[20] we estimate the difference between k and k' in that we consider local dispersion relations $f(k)$ of Fig. 4 (b). First we assume that for $H = 0$ the branch shown as the broken line is valid. For $H \neq 0$ this branch shifts to larger and smaller frequencies depending on the orientation of the magnetization vectors $\boldsymbol{M}$ in nanostripes. At $k = 0$ the two branches for opposing directions of $\boldsymbol{M}$ acquire a frequency splitting Δf_{res}. If, for a fixed excitation frequency $f > f(k = 0)$, the SW takes the wavevector $k = k_{\text{I}}$ in the MC the relevant wavevector in the SW well amounts to $k' > k_{\text{I}}$.[21] Accordingly, the transmitted spin wave experiences an extra phase shift $\Delta\Theta(H) = (k' - k_{\text{I}}) \times p = \Delta k \times p$. Based on this model, we can estimate phase shifts from independently measured parameters in that we consider

$$\begin{aligned} \Delta\Theta &= \Delta k \times p \approx (\Delta k/\Delta f_{\text{res}}) \times \Delta f_{\text{res}} \times p \\ &\approx (df/dk)^{-1} \times [(df/dH) \times 2H] \times p. \end{aligned} \quad (1)$$

From the dispersion relations of the lowest minibands (dashed green lines) in Fig. 1 (b) and (c) we evaluate the first term, i.e., the slopes $df/dk = v_{\text{g}}/2\pi$. We find 0.346 $\frac{\text{GHz } \mu\text{m}}{\text{rad}}$ (0.464 $\frac{\text{GHz } \mu\text{m}}{\text{rad}}$) for MC1 (MC2). For the second term we evaluate the curves $P1$ in $a_{21,\text{SAT}}$ of Fig. 2 (a) and (g) in that we extract the field dependency of the eigenfrequencies, df/dH, for $H < H^{*}$ and $H < H'^{*}$, respectively. We get 80 MHz/mT for MC1 and 114 MHz/mT for

MC2. We assume df/dH to be constant in the field regime defined by Fig. 3. Using these values, we calculate the frequency offset Δf_{res} between dispersion relations $f(k)$ of MC and SW well [Fig. 4 (b)] according to $\Delta f_{\text{res}} \approx (df/dH) \times 2H$. The dashed lines shown in Fig. 3 (a) and (b) reflect the calculated phase shifts based on the model of Fig. 4 and Eq. (1). The model explains the magnitude of the experimentally extracted $\Delta\Theta$ well and underlines that a modified wavevector in the magnetic defect causes an appreciable field-dependent phase shift. Equation (1) allows us to optimize the phase shift. Following Eq. (1) the phase shift depends on the product H/v_{g}. To increase $\Delta\Theta$ one needs to either reduce v_{g} or, more favourably, increase the field H^* which is applied without reversing the magnetic defect. An additional uniaxial anisotropy along the long axis of the nanostripe might allow for large H^*.

The increase of k' in the defect might also explain the observed field-dependence of relative signal strength $\eta(H)$. We think of two relevant mechanisms. First, SW reflection at the defect can occur due to the inhomogeneous H_{eff}[7], inducing a mismatch of the wave impedance[9]; second, a large wavevector reduces the dipolar strength across a gap[22]. Therefore we expect a reduced dipolar coupling for an increased k' at the defect. We note that in our experiment we intentionally used long stripes with a small demagnetization field. In the contrary, Haldar et *al.*[10] explored a chain of short nanomagnets. In this case a significant change of the demagnetization field took place when the magnetization direction of an individual nanomagnet was switched. Consistently, the authors reported a pronounced SW attenuation at a reversed nanomagnet for already $H = 0$.

To avoid the bias magnetic field H that we introduced to adjust effective fields for SW phase control, one could expose the relevant CoFeB nanostripe to a magnetic anisotropy that is induced by e.g. inverse magnetostriction[23]. If provided by a ferroelectric substrate, this anisotropy and the related H_{eff} can be controlled by an electric field[24,25]. The concept outlined here could allow for all-magnon data processing if -in a three terminal device- spin waves induce domain-wall motion in the magnetic defect[26] and thereby control the magnetization direction of the corresponding SW well through which spin waves are transmitted.

In conclusion, we demonstrated that SW amplitudes and phases are controlled via a magnetic defect in a 1D magnonic crystal. A phase shift of almost π was observed and explained by a modified wavevector at the defect forming a spin-wave well.

SUPPLEMENTARY MATERIAL

See supplementary material for a_{11} and a_{21} of MC2 for increasing H.

ACKNOWLEDGMENT

We thank for funding by SNSF via grant 163016. We thank F. Stellacci and E. Athanasopoulou for support concerning MFM.

[1] A. Khitun, M. Bao, and K. L. Wang, J. Phys. D: Appl. Phys. **43**, 264005 (2010).
[2] G. Csaba, Á. Papp, and W. Porod, Phys. Lett. A **381**, 1471 (2017).
[3] A. V. Chumak, A. A. Serga, and B. Hillebrands, J. Phys. D: Appl. Phys. **50**, 244001 (2017).
[4] R. Hertel, W. Wulfhekel, and J. Kirschner, Phys. Rev. Lett. **93**, 257202 (2004).
[5] M. P. Kostylev, A. A. Serga, T. Schneider, B. Leven, and B. Hillebrands, Appl. Phys. Lett. **87**, 153501 (2005), http://dx.doi.org/10.1063/1.2089147.
[6] T. Schneider, A. A. Serga, B. Leven, B. Hillebrands, R. L. Stamps, and M. P. Kostylev, Appl. Phys. Lett. **92**, 022505 (2008), http://dx.doi.org/10.1063/1.2834714.
[7] S. O. Demokritov, A. A. Serga, A. André, V. E. Demidov, M. P. Kostylev, B. Hillebrands, and A. N. Slavin, Phys. Rev. Lett. **93**, 047201 (2004).
[8] J. Ding, M. Kostylev, and A. O. Adeyeye, Phys. Rev. Lett. **107**, 047205 (2011).
[9] R. Huber, T. Schwarze, and D. Grundler, Phys. Rev. B **88**, 100405 (2013).
[10] A. Haldar, D. Kumar, and A. O. Adeyeye, Nat. Nano. **11**, 437 (2016).
[11] V. L. Zhang, H. S. Lim, S. C. Ng, M. H. Kuok, X. Zhou, and A. O. Adeyeye, AIP Adv. **6**, 115106 (2016), http://dx.doi.org/10.1063/1.4967334.
[12] H. Yu, R. Huber, T. Schwarze, F. Brandl, T. Rapp, P. Berberich, G. Duerr, and D. Grundler, Appl. Phys. Lett. **100**, 262412 (2012), http://dx.doi.org/10.1063/1.4731273.

[13]V. E. Demidov, M. P. Kostylev, K. Rott, P. Krzysteczko, G. Reiss, and S. O. Demokritov, Appl. Phys. Lett. **95**, 112509 (2009), http://dx.doi.org/10.1063/1.3231875.

[14]S. Demokritov, B. Hillebrands, and A. Slavin, Phys. Rep. **348**, 441 (2001).

[15]G. Gubbiotti, S. Tacchi, G. Carlotti, N. Singh, S. Goolaup, A. O. Adeyeye, and M. Kostylev, Appl. Phys. Lett. **90**, 092503 (2007), http://dx.doi.org/10.1063/1.2709909.

[16]M. Bailleul, D. Olligs, and C. Fermon, Appl. Phys. Lett. **83**, 972 (2003), http://dx.doi.org/10.1063/1.1597745.

[17]C. S. Chang, M. Kostylev, E. Ivanov, J. Ding, and A. O. Adeyeye, Appl. Phys. Lett. **104**, 032408 (2014), http://dx.doi.org/10.1063/1.4863078.

[18]S. Neusser, G. Duerr, H. G. Bauer, S. Tacchi, M. Madami, G. Woltersdorf, G. Gubbiotti, C. H. Back, and D. Grundler, Phys. Rev. Lett. **105**, 067208 (2010).

[19]A. Gurevich and G. Melkov, *Magnetization Oscillations and Waves* (Taylor & Francis, 1996).

[20]C. Bayer, S. O. Demokritov, B. Hillebrands, and A. N. Slavin, Appl. Phys. Lett. **82**, 607 (2003), http://dx.doi.org/10.1063/1.1540734.

[21]For the sketch in Fig. 4 (b) we assumed that branches differed by a constant $\Delta f = \Delta f_{\text{res}}$ for all k as H was small compared to M.

[22]T. Schneider, A. A. Serga, A. V. Chumak, B. Hillebrands, R. L. Stamps, and M. P. Kostylev, EPL (Europhysics Letters) **90**, 27003 (2010).

[23]S. J. Hämäläinen, F. Brandl, K. J. A. Franke, D. Grundler, and S. van Dijken, Phys. Rev. Appl. **8**, 014020 (2017).

[24]B. Botters, F. Giesen, J. Podbielski, P. Bach, G. Schmidt, L. W. Molenkamp, and D. Grundler, Appl. Phys. Lett. **89**, 242505 (2006), http://dx.doi.org/10.1063/1.2405885.

[25]S. Cherepov, P. K. Amiri, J. G. Alzate, K. Wong, M. Lewis, P. Upadhyaya, J. Nath, M. Bao, A. Bur, T. Wu *et al.*, Appl. Phys. Lett. **104**, 082403 (2014), http://dx.doi.org/10.1063/1.4865916.

[26]M. Krawczyk and D. Grundler, J. Phys.: Condens. Matter **26**, 123202 (2014).

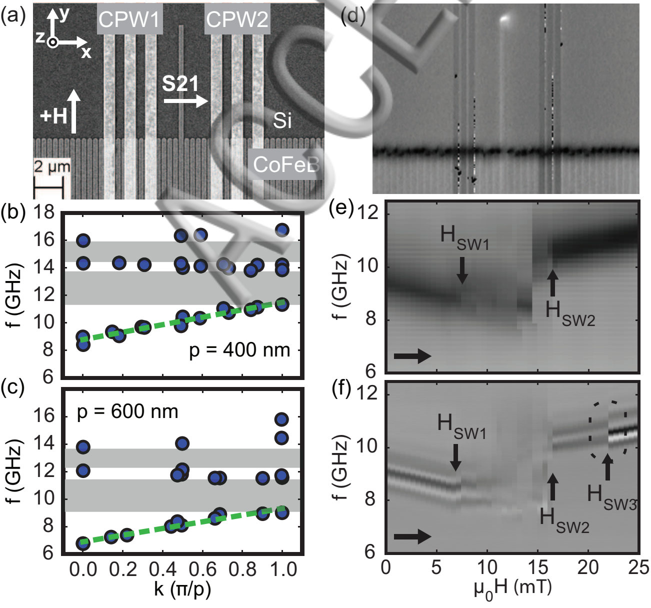

(a)
y
z
x
CPW1
CPW2
S21
+H
Si
CoFeB
2 μm
(d)
(b)
f (GHz)
p = 400 nm
(c)
p = 600 nm
k (π/p)
(e)
H_SW1
H_SW2
f (GHz)
(f)
H_SW1
H_SW2
H_SW3
μ_0H (mT)

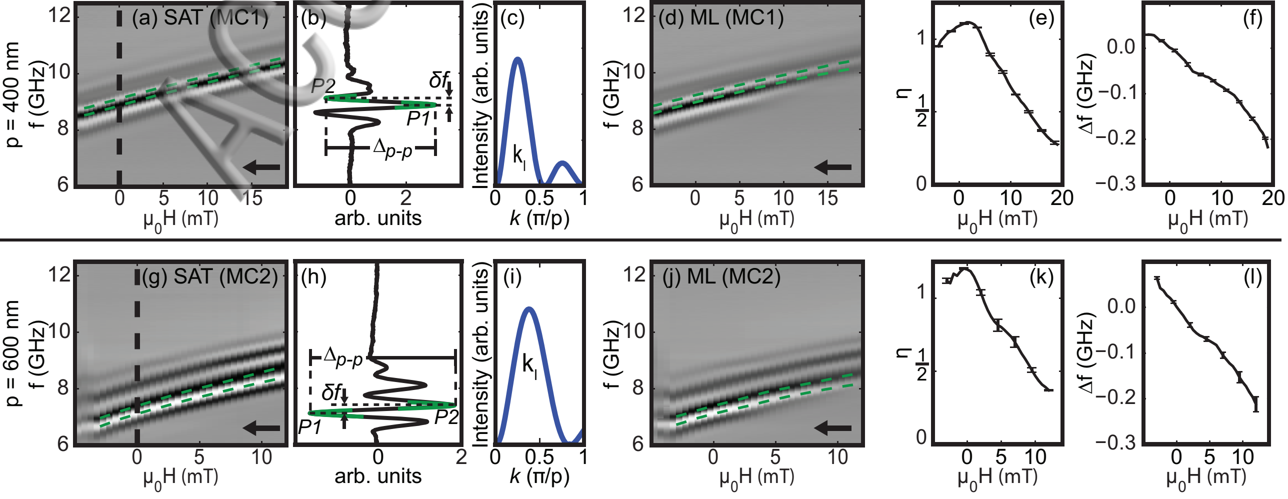

p = 400 nm
(a) SAT (MC1)
(b)
P2
δf
P1
Δp-p
(c)
Intensity (arb. units)
k
(d) ML (MC1)
(e)
η
(f)
Δf (GHz)
f (GHz)
μ0H (mT)
arb. units
k (π/p)
p = 600 nm
(g) SAT (MC2)
(h)
(i)
(j) ML (MC2)
(k)
(l)

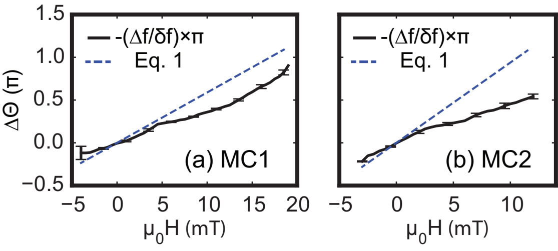

-(Δf/δf)×π
Eq. 1
(a) MC1
-(Δf/δf)×π
Eq. 1
(b) MC2
ΔΘ (π)
μ0H (mT)
μ0H (mT)
1.5
1.0
0.5
0.0
−0.5
−5
0
5
10
15
20
−5
0
5
10

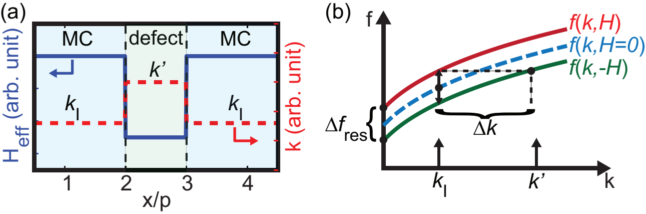

(a)
MC
defect
MC
k'
k_l
k_l
H_{eff} (arb. unit)
k (arb. unit)
1
2
3
4
x/p
(b)
f
f(k,H)
f(k,H=0)
f(k,-H)
Δf_{res}
Δk
k_l
k'
k